



A novel identification technique of machine tool support stiffness under the variance of structural weight

Zhen-Wei Zhuang¹ · Jen-Chang Lu¹ · De-Shin Liu¹

Received: 28 May 2021 / Accepted: 18 October 2021 / Published online: 28 October 2021
© The Author(s) 2021

Abstract

The preload-dependent stiffness of machine tool support was investigated in this study. A novel identification method of support stiffness has been proposed through the experimental modal analysis and finite element method. The support stiffness was identified with different machine weight during the assembling process of a machining center. Specifically, the structure weight increase of a machine tool in the assembly process causes its center of gravity to shift. Accordingly, the variance of support reaction affects the support stiffness. To explore the variance of support stiffness, the researchers of this study collaborated with a machine tool manufacturer. Impact testing was performed on each assembly stage. Additionally, finite element analysis was used to establish equations between the reaction force versus stiffness of supports under the structural weight variance. The obtained equations were used to predict the natural frequency and vibration mode of structures in various assembly stages. The maximum error between the experimental and simulated natural frequencies was 7.1%, and the minimum modal assurance criterion was 0.77. Finally, a modal analysis model that updates support stiffness automatically, which could be adopted by machine builders to develop new machine tool, is proposed.

Keywords Machine tool design · Variance of support stiffness · Natural frequency · Modal analysis · Finite element analysis

1 Introduction

The trial-and-error method was a technique commonly used in machine design; now, virtual prototyping technology is increasingly adopted to reduce the development cost and time of machine tool builders [1]. In particular, finite element analysis (FEA) has been widely applied in machine design [2–5]. Garitaonandia et al. [6, 7] used FEA to analyze grinding machines, determine machining chatter, and predict the position-dependent dynamic behavior of a machine. Liang et al. [8] optimized the design and dynamic performance of an ultraprecision machine tool. Shen et al. [9] used FEA to identify structural weaknesses of a machine and optimized the machine's dynamic characteristics through topology optimization. Accurate prediction of the vibration characteristics (including natural frequencies

and mode shapes) of machines is critical at the design stage because it prevents workpiece defects caused by machining vibrations. In the simulation of dynamic characteristics for an assembled machine tool, joint interface characteristics are the most crucial information, apart from geometry and material properties. Various studies have investigated the stiffness of joint units, including linear guideways, ball screws, and bearings, in the machine tool. Lin et al. [10] developed a finite element (FE) model to discuss the effect of the preload of linear guideways on the dynamic stiffness of a spindle, Brecher et al. [11] conducted a comprehensive study on joint constraints, and Ealo et al. [12] examined the joint stiffness of linear guideways for the industrial milling machines. Support stiffness has a direct influence on the lowest frequency of a machine. It involves a much higher level of complexity than does the stiffness of joint units and is more difficult to determine its value compared with motion component stiffness; therefore, some studies have overlooked support stiffness in their FEA-based machine design [13–20]. Disregarding support stiffness would lead to distorted modal simulations. To address this problem, scholars have researched support stiffness. Kono et al. [21] obtain

✉ Jen-Chang Lu
etet006@msn.com

¹ Department of Mechanical Engineering and Advanced Institute of Manufacturing With High-Tech Innovations, National Chung Cheng University, Chiayi, Taiwan

the interface contact stiffness between two simple different material models through a static stiffness test. After that, the contact stiffness of support was calculated to estimate the modal analysis of the whole machine. The maximum difference between the experimental and simulation results was 55%. Kono et al. [22] had also established guidelines for determining the positions of a machine’s supports as well as obtained the maximum fundamental frequency of a machine. The load cell is required to acquire data in static stiffness test. It is difficult to set the load cell directly on the support of the whole machine, which will cause more uncertainty of the boundary conditions. Therefore, this study proposes a novel method to identify the stiffness of the support, which does not require a load cell and can effectively predict the natural frequency and vibration mode under the variance of structural loading. This method performs impact testing at each stage of a machine tool builder’s assembly process and the modal finite element modeling was validated to construct accurate equations between support stiffness and reaction force.

This study is organized as follows. Section 2 introduces the machine used in the experiment and the experimental methods. Section 3 verifies and simulates the material properties of castings, conducts a modal analysis for each assembly stage, compares the results with the experimental results for verification, and constructs equations for support contact stiffness for each assembly stage. Section 4 predicts natural

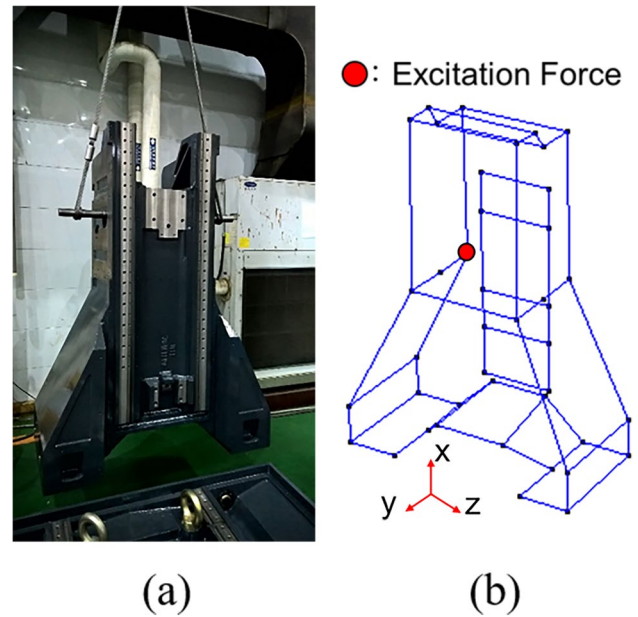


Fig. 2 Experiment on the column. a Experimental model. b EMA model

frequency and mode shape on the basis of support stiffness. Section 5 discusses the results.

2 Experimental methods and procedures

This study employed impact testing in conjunction with the experimental modal analysis (EMA) and excited a machine structure with an impact hammer to elicit the structure’s natural frequency. The experiment was conducted by moving an accelerometer to each measurement point and applying impact on a fixed point at different directions. Three impacts were applied on each measurement point to collect three signals, which were averaged to reduce experimental error.

Table 1 Equipment parameters for impact testing

Name	Type	Sensitivity	Unit
Impact hammer	PCB 086D20	0.2237	mV/N
Accelerometers (X)	ICP 356A02	9.76	mV/g
Accelerometers (Y)		9.86	mV/g
Accelerometers (Z)		9.68	mV/g

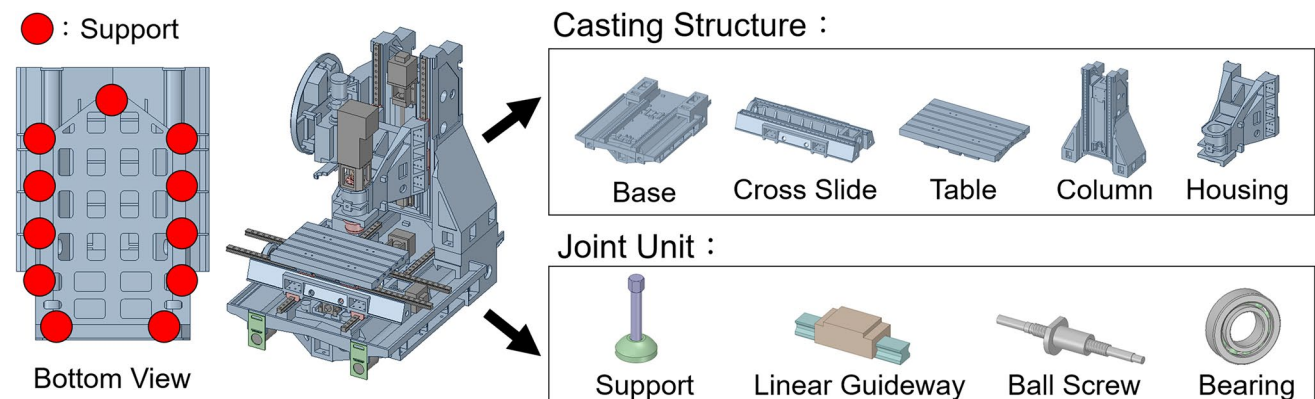


Fig. 1 Components of the vertical machining center

Table 2 Number of measuring points for casting structure

	Number of measuring points
Base	42
Cross slide	56
Table	20
Column	42
Housing	20

Table 3 Number of EMA measurement points, weight, and centers of gravity of the machine

Stage	Number of measuring points	Weight (kg)	Centers of gravity (mm)		
			X	Y	Z
1st	29	2103	744.9	970.6	267.3
2nd	41	2580	742.7	1105.1	331.8
3rd	50	2848	743.9	1157.2	374.3
4th	64	4216	743.5	918.9	677.8
5th	88	4687	743.2	936.2	759.5
6th	131	5316	771.8	941.9	838.7

Table 1 provides specifications for the equipment used in the impact testing. The measurements of frequency ranges from 0 to 150 Hz. As shown in the left side of Fig. 1, a vertical machining center that weighed 5300 kg and had 11 supports was used. For accurate simulation of machine tools, which involve complex systems, the right side of Fig. 1 shows that the machine was disassembled into two parts: (1) casting structures, which contained structural components including the base, cross slide, table, column, and housing, and (2) joint units, which comprise joint interfaces such as the supports, linear guideway, ball screw, and bearing. Each casting structure was hung for impact testing to obtain the dynamic characteristics of the machine. Take the column for example.

The column was hung as shown in Figs. 2a, b presents the measurement points for the impact testing. The number of measurement points for the casting structure is shown in Table 2. Then, the testing results were compared with those obtained in the FE modal analysis to determine the material properties of the structure. The details of the comparison are provided in Section 3.1.

Regarding the joint unit, various studies have researched the properties of linear guideways, ball screws,

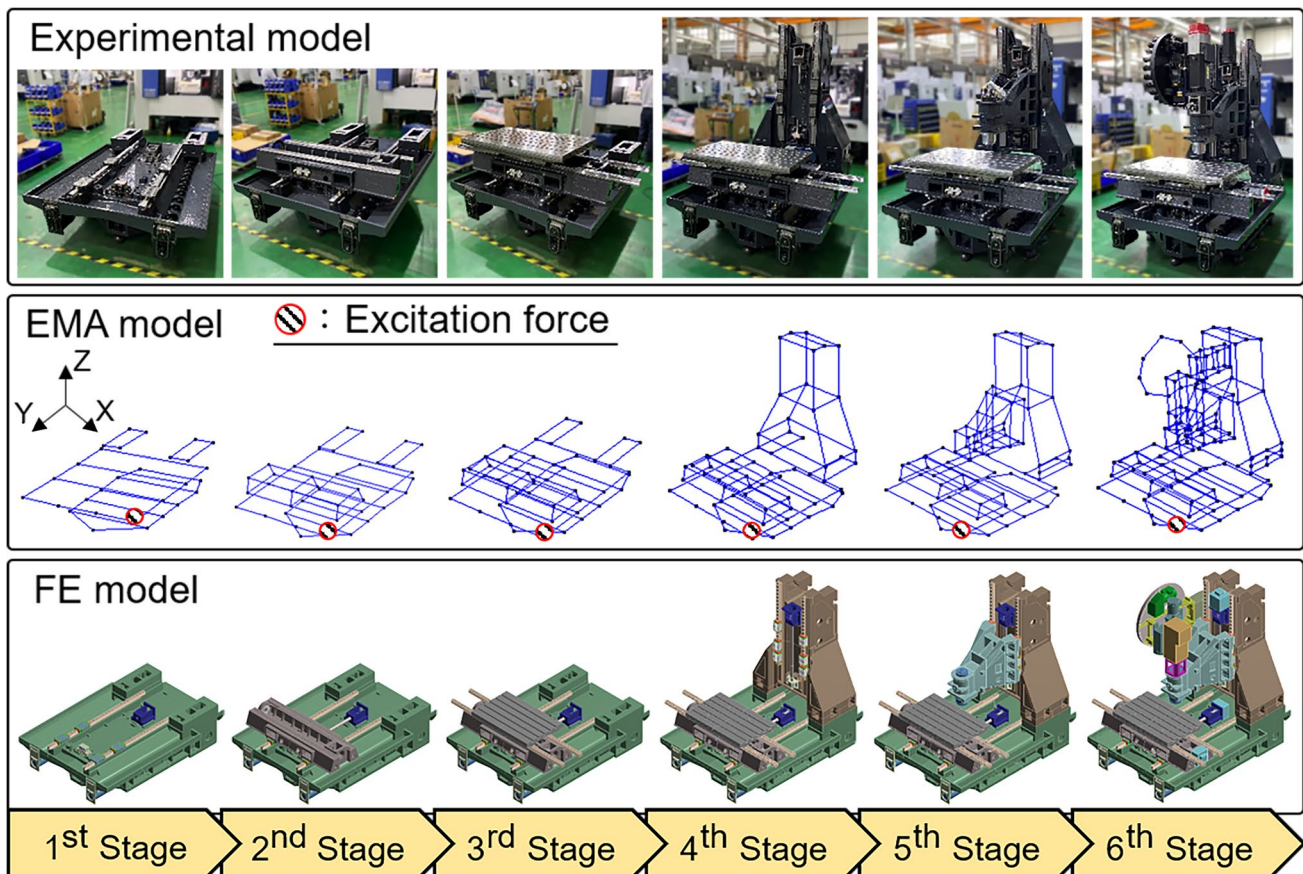


Fig. 3 Experimental, Experimental Modal Analysis, and FE model at each stage of the machine’s assembly process

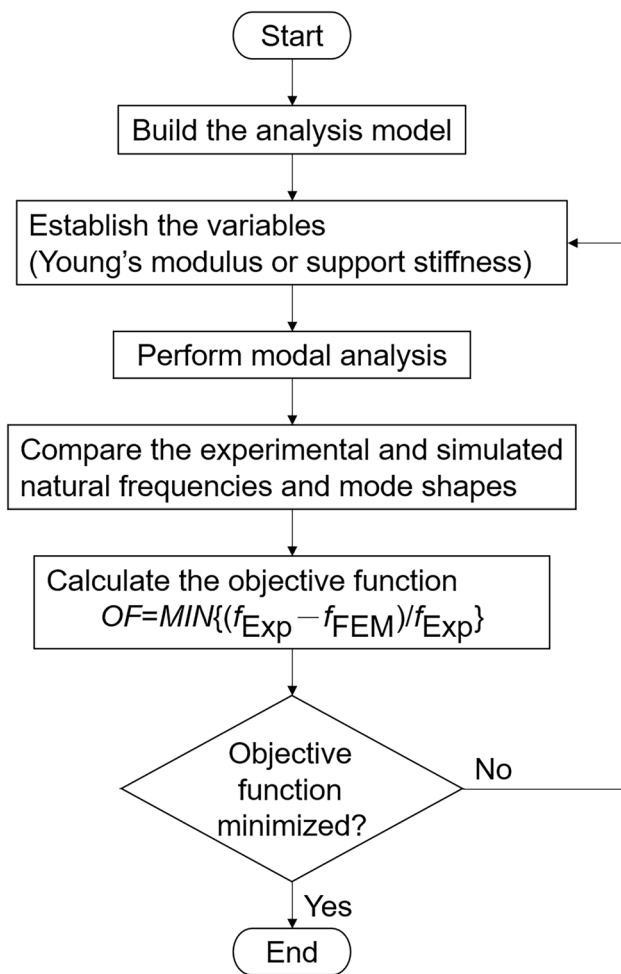


Fig. 4 Reverse finding numerical method

and bearings [23–30]. Focusing on support stiffness, the present study revealed the dynamic characteristics of the machine structure by conducting impact testing at each stage of the machine’s assembly process. The support stiffness at each stage through FEA was analyzed, and the equations for support stiffness were established. The corresponding results were presented in Section 3.2. Figure 3 describes the assembly process and points of impact on the base. The assembly process comprised six stages. In the first stage, the base was placed on the floor, supported with 11 supports, and aligned to a horizontal position. The second stage involved adding the joint unit and cross slide to the part built in the first stage. Different components were added in subsequent stages until the machine was completely assembled at the sixth stage. The measurement points for each assembly stage are presented in Table 3. The experimental results are discussed and used to verify the simulated results in Section 3.2.



Fig. 5 The weight measurement of the column

Table 4 Number of elements and nodes for each casting structure

	Table	Base	Cross slide	Column	Housing
Nodes	49,625	210,154	69,521	152,927	60,836
Elements	28,330	104,713	39,042	85,810	33,497

3 Simulation analysis and result verification

This study adopted the reverse finding numerical method as shown in Fig. 4 to determine Young’s modulus and support stiffness of the machining center according to the following process. Step 1: Establish the variables (e.g., Young’s modulus or support stiffness). Step 2: Conduct a modal analysis.

Step 3: Compare the experimental and simulated natural frequency, with the experimental natural frequency as the objective value. The objective function (OF) is defined as follows:

$$OF = MIN\{(f_{Exp} - f_{FEM})/f_{Exp}\} \tag{1}$$

where f_{Exp} is the experimental natural frequency and f_{FEM} is the FE-simulated natural frequency. The optimization was conducted using a Multi-Objective Genetic Algorithm. If the error was excessively large, the variables were modified. The reverse finding numerical method continued until the error was less than 10%.

3.1 Verification for casting materials

Researchers must ensure that the dynamic characteristics, including natural frequency and mode shape, of each casting structure are accurate before proceeding to the next assembly stage, and these characteristics are affected by structural geometry and material properties. Accordingly, three-dimensional computer-aided design models should be modified in accordance with the actual structural geometry of the machines. The geometry of FEA must be accurately modeled and it is assumed that the material of each part is homogeneous. The material properties of each casting structure for FE model were identified through the following steps. First, each casting structure was weighed as shown in Fig. 5 to obtain the actual weight, and the actual weight was divided by the geometric volume to obtain the structural density. Second, Young’s modulus was obtained through the reverse finding numerical method as shown in Fig. 4. The first three structural natural frequencies obtained in the impact testing were considered as the objective value, with Young’s modulus as the variable. The objective function as listed in Eq. (1) was solved to minimize the error between the experimental and simulated results. This study compared the experimental and simulated mode shapes using the modal assurance criterion (MAC) [31]. The obtained result was the equivalent Young’s modulus, and the Poisson’s ratios were all 0.29. FE models were constructed using ANSYS software, and the number of nodes and elements for each casting structure model is shown in Table 4. Table 5 shows that the maximum difference between the experimental and simulated frequencies was observed to be 5.3%, and the minimum MAC was 0.77. Figure 6 reveals the first three experimental and simulated mode shapes of the base. Due to its unconstrained boundaries, the base exhibited flexible-body modes in both the experimental and simulated results. The identified material properties in Table 6 were used for subsequent analysis; FC250 was the material used for the

Table 5 Comparison between the experimental and simulated natural frequencies and MAC for the casting structures

Casting Structure	Frequency (Hz)			
	Mode	1	2	3
Table	Experiment	255	438	584
	FEA	249	435	579
	Error (%)	2.4	0.7	0.9
	MAC	0.91	0.93	0.77
Base	Experiment	131	218	239
	FEA	138	219	239
	Error (%)	5.3	0.5	0.0
	MAC	0.96	0.91	0.94
Cross slide	Experiment	250	332	516
	FEA	241	331	518
	Error (%)	3.6	0.3	0.4
	MAC	0.97	0.82	0.90
Column	Experiment	204	382	422
	FEA	204	380	424
	Error (%)	0	0.5	0.5
	MAC	0.99	0.86	0.94
Housing	Experiment	663	842	908
	FEA	631	865	905
	Error (%)	4.8	2.8	0.3
	MAC	0.96	0.85	0.84

table, and FC300 was used for the base, cross slide, column, and housing. Young’s modulus of FC300 was greater than that of FC250, which verified that the material parameters were reliable.

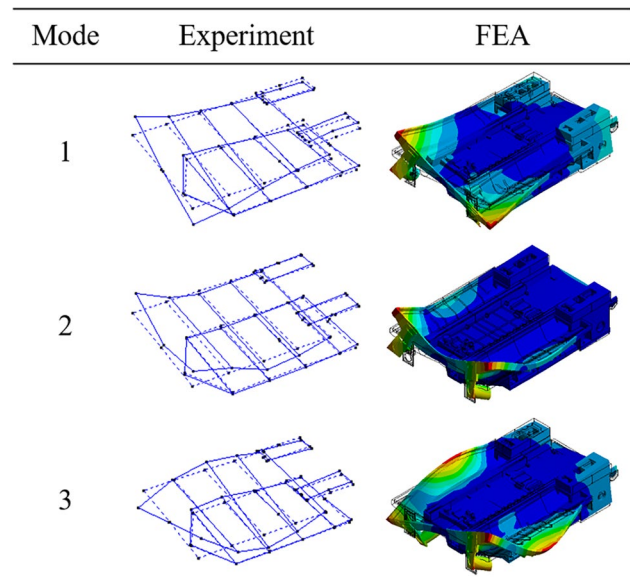


Fig. 6 Experimental and FEA mode shapes of the base

Table 6 Material properties

	Table	Base	Cross slide	Column	Housing
Material	FC250	FC300	FC300	FC300	FC300
Density (kg/m ³)	7358	8304	7475	7368	7743
Young's modulus (GPa)	133	172	141	146	167
Poisson's ratio	0.29	0.29	0.29	0.29	0.29
Weight (kg)	265	1980	380	1290	410

3.2 Reversal numerically finding of support stiffness at each assembly stage

The assembly of the whole machine in FEA is connected by settings including support joint, fixed joint,

linear guide, and feed drive, as shown in Fig. 7. Support joint is set between base and floor. Regarding the 11 supports of the machine, the floor, supports, and bolts were replaced by spring elements with three degrees of freedom as shown in Fig. 8. Each one of the supports

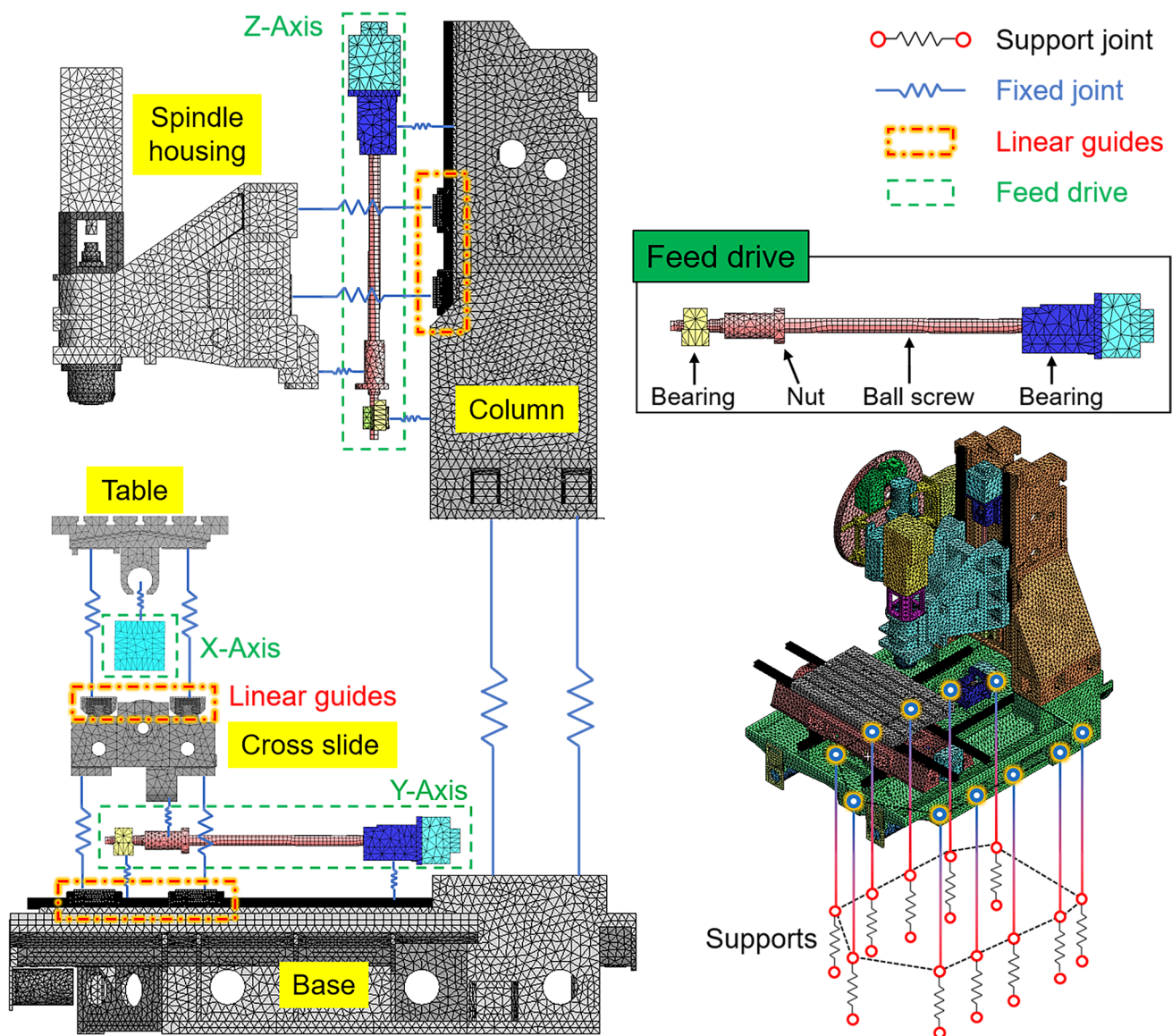


Fig. 7 Modeling of the whole machine

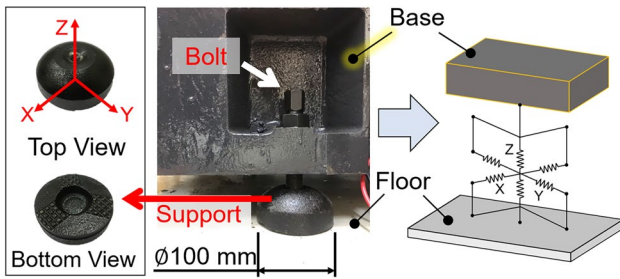


Fig. 8 Simplification settings for supports

has three-directional stiffness, namely x -, y -, and z -directions. Because the area of the support bottom that came into contact with the floor was round, the stiffness in the horizontal directions (i.e., the x - and y -directions) was considered identical. Fixed joints are set at the parts connected with the tightening bolts, such as the contact interfaces between the base and the column. The connection is highly rigid, so it is regarded as a continuous structure. Due to the excessively large number and small size of balls and rollers in the ball screws, bearings, and linear guideways, the balls and rollers were replaced with spring elements with three degrees of freedom in the simulation, as shown in Fig. 9A. The spring elements in the linear guide are between rail and block, as shown in Fig. 9B. The feed drive system contains bearings and ball screws. The spring elements are used to link the screw and the nut for the ball screws (Fig. 9C) and the inner and the outer rings for the bearing (Fig. 9D), respectively.

Table 7 Numbers of nodes and elements for each assembly stage

Stage	1st	2nd	3rd	4th
Nodes	591,618	1,053,313	1,104,088	1,620,364
Elements	644,869	1,247,492	1,277,029	1,894,493

Table 7 illustrates the number of nodes and elements of the FE model at each assembly stage. The support stiffness was obtained through the reverse finding numerical method as shown in Fig. 4. The support stiffness is ranged from 10^3 to 10^6 N/mm according to the reference [21, 22]. Therefore, the initial value, 1×10^5 N/mm, will be used to optimize the support stiffness. The first three structural natural frequencies obtained in the impact testing were considered as the objective value, with the support stiffness as the variable. The objective function as listed in Eq. (1) was solved to minimize the error between the experimental and simulated results. The comparison between the experimental and FE-simulated natural frequencies are shown in Table 8. Since the stiffness of the support is sensitive at the lowest natural frequency, only the first three modes are discussed in this study. The maximum difference between the experimental and FE-simulated frequencies was 6.9%, and the minimum MAC was 0.7. According to the first assembly stage as shown in Fig. 10, the base, when placed on the floor, had an additional rigid-body mode compared with the unconstrained boundary model shown in Fig. 6 and was accurately simulated.

Fig. 9 Simplification settings for joint units

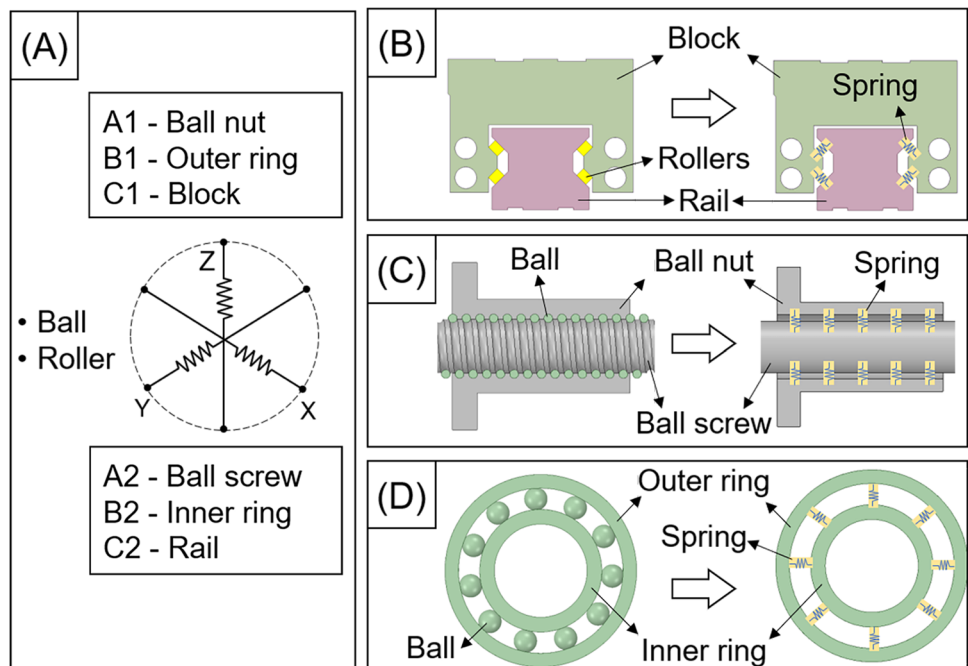


Table 8 Comparison between the experimental and simulated natural frequencies and MAC for the 1st–4th stage (unit: Hz)

Stage	Mode	1	2	3
1st	Experiment	54	63	98
	FEA	52.4	58.7	96.8
	Error (%)	2.9	6.9	1.2
	MAC	0.78	0.94	0.7
2nd	Experiment	45.5	57	88
	FEA	46.2	55	86.8
	Error (%)	1.4	3.6	1.3
	MAC	0.98	0.79	0.72
3rd	Experiment	44.5	53.5	88.5
	FEA	47.6	55.1	86.8
	Error (%)	6.9	3.0	1.9
	MAC	0.94	0.9	0.75
4th	Experiment	34	46	75.5
	FEA	36.1	48.1	76.6
	Error (%)	6.1	4.6	1.4
	MAC	0.7	0.97	0.9

4 Experimental verification of the stiffness model

4.1 Support stiffness equation

According to Fig. 11 and Table 3, the machine’s center of gravity and weight changed as the assembly process proceeded. Therefore, a static analysis was used to obtain the

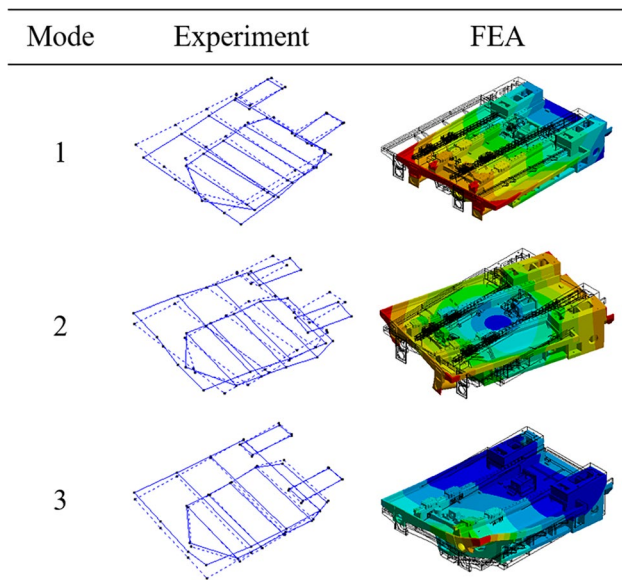


Fig. 10 Experimental and simulated mode shapes for the first assembly stage

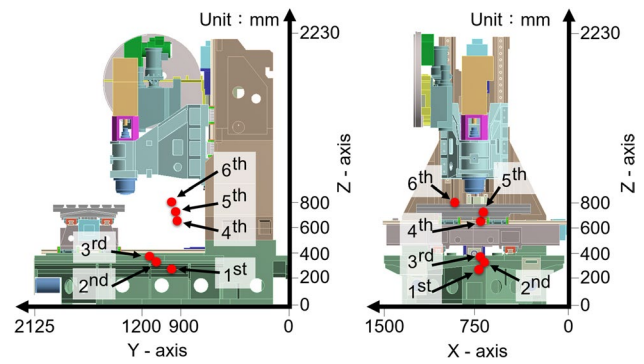


Fig. 11 Distribution of the centers of gravity at different assembly stages

support reaction force at each assembly stage. The identified support stiffness and reaction force from the first to fourth stage were then categorized in relation to the vertical and horizontal directions, and the least squares method was used to identify the relationship between support stiffness and reaction force as shown in Fig. 12. The equations for the support stiffness and the reaction force are established as follows:

$$K_v = -0.0058F^2 + 105.08F - 98761 \tag{2}$$

$$K_h = -0.0003F^2 + 5.41F + 13671 \tag{3}$$

where F denotes the support reaction force, K_v the vertical support stiffness, and K_h the horizontal support stiffness. Equation (2) is the equation between the support reaction force and stiffness in the vertical direction. Equation (3) is the equation between the support reaction force and stiffness

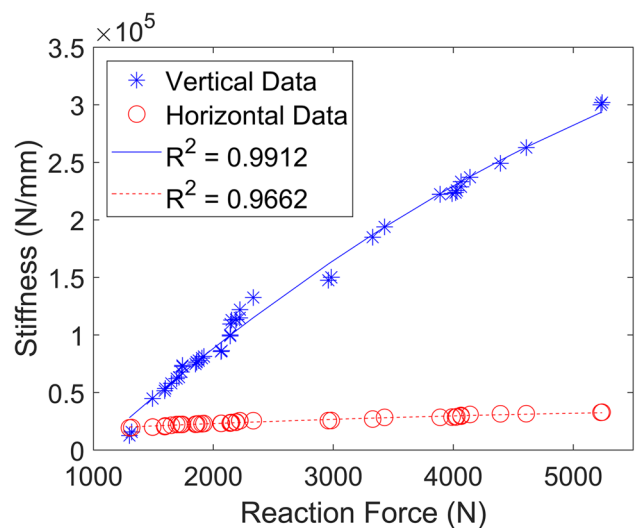


Fig. 12 Support stiffness and reaction force in the vertical and horizontal direction

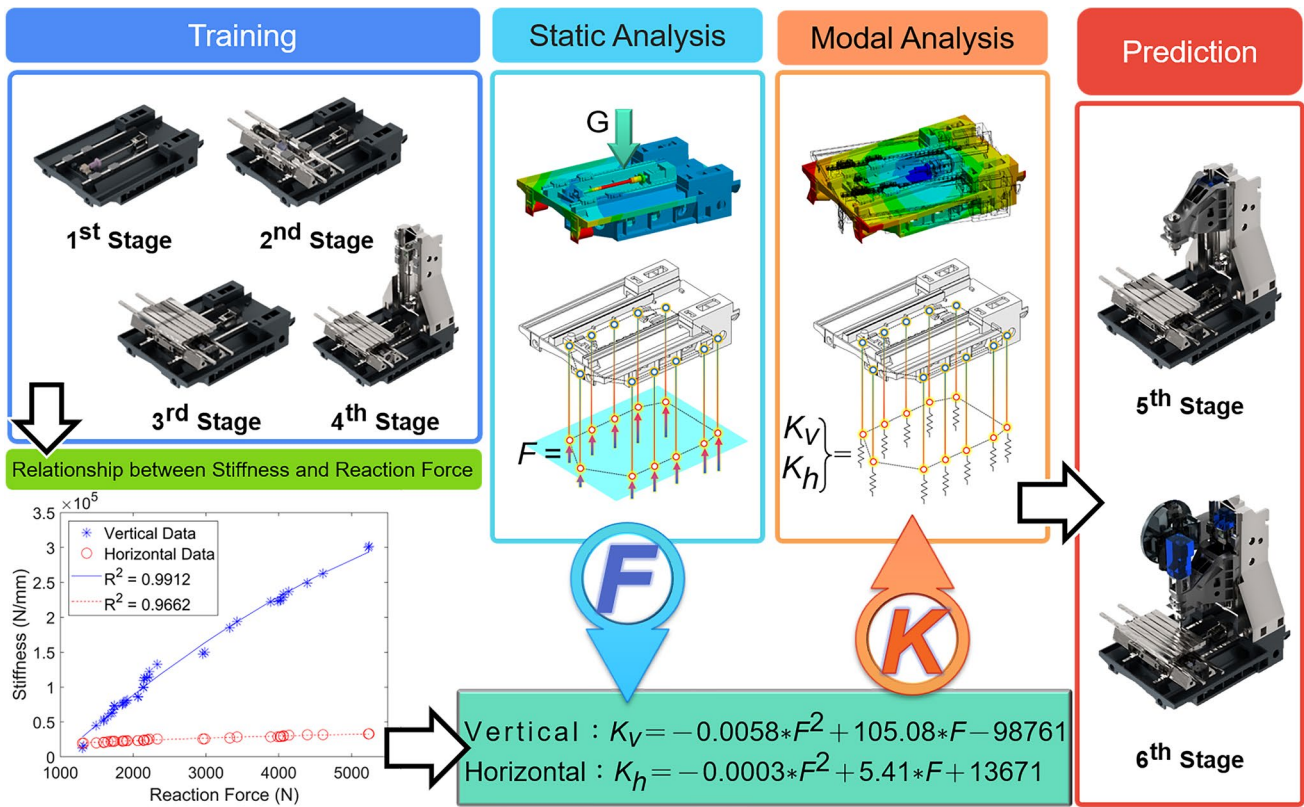


Fig. 13 Process for applying stiffness equations in dynamic characteristic prediction

in the horizontal direction. According to the above equations, support stiffness grows as the support reaction force increases. In Section 4.2, the proposed equations are used to predict the dynamic characteristics of the structural characteristics in the fifth and sixth assembly stages, and the FE simulated analysis is experimentally verified.

4.2 Application of support stiffness equations

To verify the feasibility of the equations for support established according to the first four assembly stages, the equations were used to predict the natural frequencies and mode shapes in the final two assembly stages. The process is depicted in Fig. 13. A modal finite element model that updates support stiffness automatically is proposed. A static analysis was first performed to obtain the reaction force on each support when gravity was applied to the entire structure

Table 9 Numbers of nodes and elements for each assembly stage

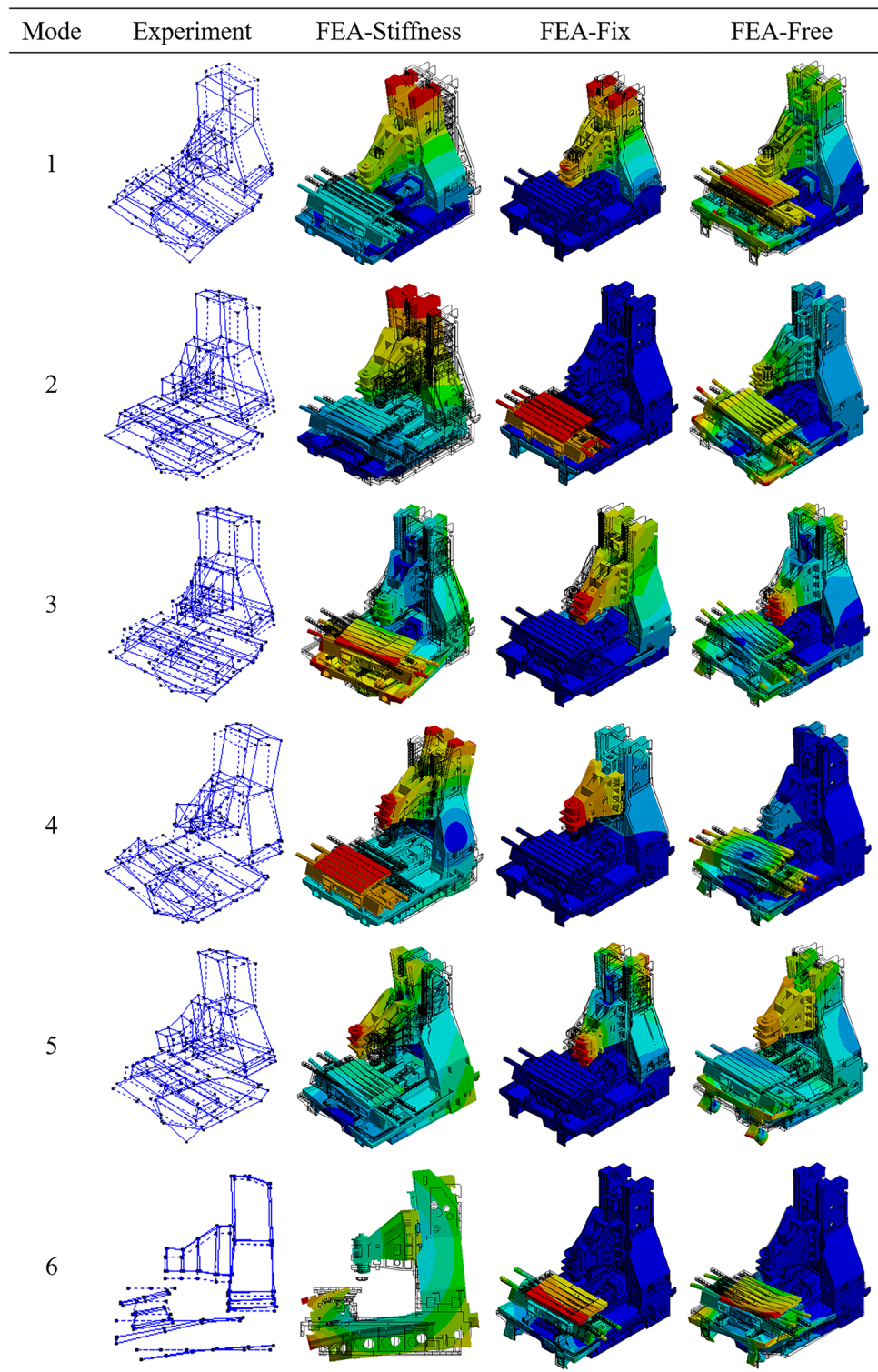
Stage	5th	6th
Nodes	1,686,467	1,698,175
Elements	1,944,168	1,985,549

of the machine. Then, the reaction force was substituted into Eqs. (2) and (3) to calculate the stiffness of each support, which was then substituted into the modal analysis. The natural frequencies and mode shapes were finally compared between experimental and FEA simulated results. Table 9 presents the number of nodes and elements for the FE model in each assembly stage. Table 10 shows that the maximum difference between the experimental and simulated natural frequencies was 7.1%, and the minimum MAC was 0.77. Figure 14 reveals the experimental and simulated mode shapes for the fifth stage.

Table 10 Comparison between experimental and simulated natural frequencies and MAC (unit: Hz)

Stage	Mode	1	2	3
5th	Experiment	30.5	32	43
	FEA-Stiffness	32.5	34.3	44.5
	Error (%)	6.5	7.1	3.6
	MAC	0.77	0.93	0.98
6th	Experiment	26.5	31.5	44
	FEA-Stiffness	25.9	33.6	43.6
	Error (%)	2.2	6.6	0.9
	MAC	0.77	0.93	0.91

Fig. 14 Comparison of the mode shape in the fifth stage between the FEA-Stiffness, FEA-Fix, and FEA-Free models



In order to explain the importance of the stiffness of the support clearly, the models with fixed (FEA-Fix) and unconstrained (FEA-Free) boundary conditions for the support were presented for comparison with the experimental results. The mode shapes in Fig. 14 include rigid body modes and flexible body modes. The joint stiffness, including that of the

linear rail, screw, and bearing, was considered in the above analysis model, and hence, the result indicates the relative mode shape. As shown in Fig. 14, the fourth mode of FEA-Free was the torsional mode of the cross slide and table.

The error and MAC were calculated on the basis of an experiment. Table 11 and Fig. 14 show that the maximum

Table 11 Comparison between experimental and simulated natural frequencies and MAC for different boundary conditions (Unit: Hz)

Stage	Mode	1	2	3	4	5	6
5th	Experiment	30.5	32	43	56	82.5	91
	FEA-Stiffness	32.5	34.3	44.5	60.6	82.7	91.7
	Error (%)	6.5	7.1	3.6	8.2	0.2	0.8
	MAC	0.77	0.93	0.98	0.78	0.91	0.75
	FEA-Fix	59.5	75.6	90.0	105.6	110.9	111.7
	Error (%)	95	136	109	89	34	23
	MAC	0.45	0.07	0	0.05	0.23	0.27
	FEA-Free	65.6	76.4	117.3	132.1	135.3	155.5
	Error (%)	115	139	173	136	64	71
	MAC	0	0.01	0.02	0.11	0.02	0.07

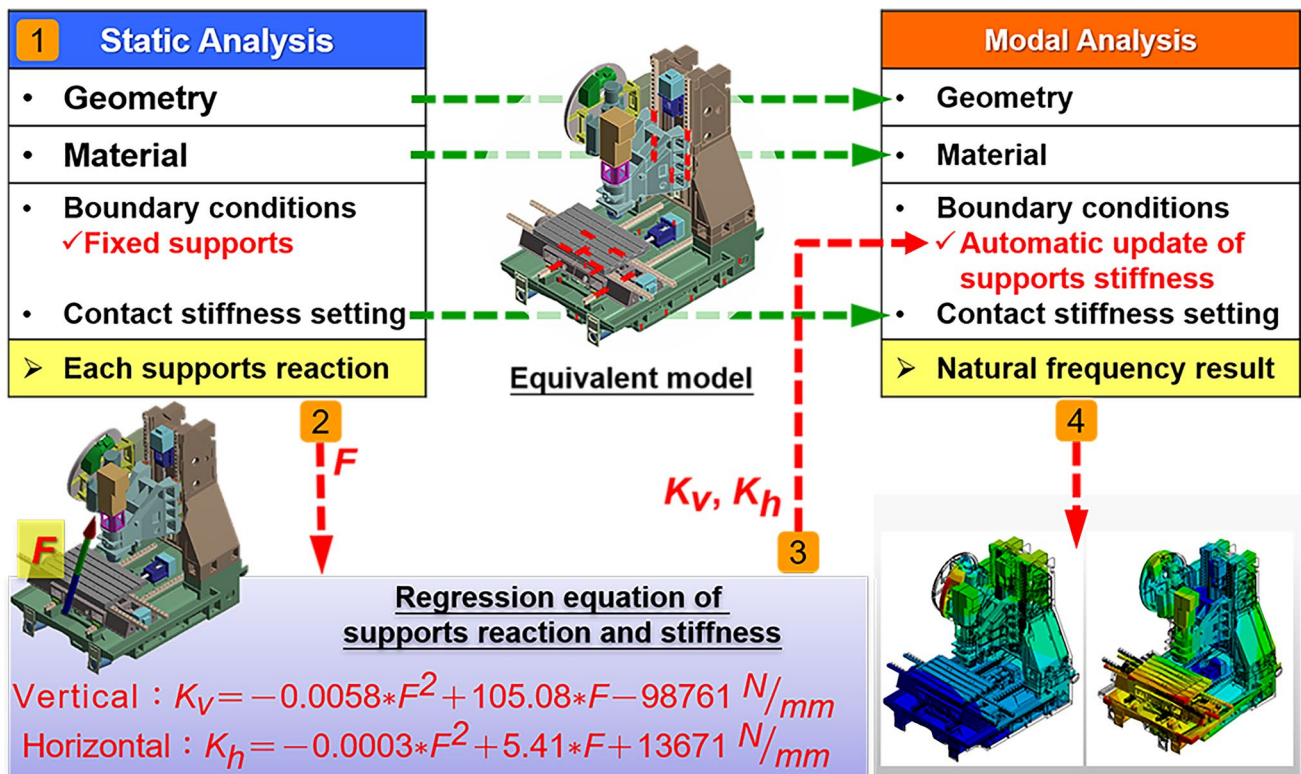


Fig. 15 Modal analysis model updating support stiffness automatically

frequency difference was 136%, and the MAC value was close to 0.45 for the fixed support conditions (FEA- Fix). Because the support was fixed, the base was stationary in the overall mode shape; the maximum frequency difference was 173%, and the MAC value was close to 0.11 for the unconstrained support conditions (FEA-Free). The above two models showed that the consideration of support stiffness could increase the accuracy of the finite element model of the full machine. According to the aforementioned process, the proposed equations for support stiffness and reaction force can be used to predict vibration characteristics of machines at different assembly stages.

5 Conclusion

The proposed research process facilitated effective establishment of equations between the reaction force and the stiffness of a machine’s supports. The study also constructed a modal analysis model as shown in Fig. 15 able to update support stiffness automatically from the static FE-model, produce results consistent with those of the EMA, and predict the natural frequencies and mode shapes of a different structural mechanism. In conventional machine design, the settings of support stiffness are unknown to machine

builders. Therefore, the research results could provide machine builders with insights into the development of new machines and enable prediction of a machine's modal changes when its weight changes due to changes in its structure, such as modifying the 3-axis machine tools to four or five axes machine.

Author contribution Zhen-Wei Zhuang: conceptualization, methodology, investigation, data curation, writing—original draft, writing—review & editing, visualization, supervision. Jen-Chang Lu: conceptualization, methodology, software, validation, formal analysis, investigation, data curation, writing—original draft, writing—review & editing, visualization. De-Shin Liu: conceptualization, resources, writing—review & editing, supervision, project administration, funding acquisition.

Funding This work was partially supported by the Advanced Institute of Manufacturing with High-tech Innovations (AIM-HI) from The Featured Areas Research Center Program within the framework of the Higher Education Sprout Project by the Ministry of Education (MOE) in Taiwan. The current authors also gratefully acknowledge the financial support provided to this study by the Ministry of Science and Technology, Taiwan, R. O. C., under Grant Nos. MOST110-2634-F-194-003 and MOST110-2634-F-194-005.

Data availability The data is a part of an ongoing study and cannot be shared at this particular moment.

Code availability Commercial FEA software ANSYS.

Declarations

Conflict of interest The authors declare no competing interests.

Open Access This article is licensed under a Creative Commons Attribution 4.0 International License, which permits use, sharing, adaptation, distribution and reproduction in any medium or format, as long as you give appropriate credit to the original author(s) and the source, provide a link to the Creative Commons licence, and indicate if changes were made. The images or other third party material in this article are included in the article's Creative Commons licence, unless indicated otherwise in a credit line to the material. If material is not included in the article's Creative Commons licence and your intended use is not permitted by statutory regulation or exceeds the permitted use, you will need to obtain permission directly from the copyright holder. To view a copy of this licence, visit <http://creativecommons.org/licenses/by/4.0/>.

References

- Altintas Y, Brecher C, Weck M, Witt S (2005) Virtual machine tool. *CIRP Ann* 54:115–138. [https://doi.org/10.1016/S0007-8506\(07\)60022-5](https://doi.org/10.1016/S0007-8506(07)60022-5)
- Huang DTY, Lee JJ (2001) On obtaining machine tool stiffness by CAE techniques. *Int J Mach Tools Manuf* 41:1149–1163. [https://doi.org/10.1016/S0890-6955\(01\)00012-8](https://doi.org/10.1016/S0890-6955(01)00012-8)
- Kolar P, Sulitka M, Janota M (2011) Simulation of dynamic properties of a spindle and tool system coupled with a machine tool frame. *Int J Adv Manuf Technol* 54:11–20. <https://doi.org/10.1007/s00170-010-2917-7>
- Zhang L, Ma L, Wu D, Zhou Y (2019) A novel integrated process-machine approach for designing customized milling machines. *Int J Adv Manuf Technol* 104:245–260. <https://doi.org/10.1007/s00170-019-03742-x>
- Ji Q, Li C, Zhu D, Jin Y, Lv Y, He J (2020) Structural design optimization of moving component in CNC machine tool for energy saving. *J Cleaner Prod* 246:118976. <https://doi.org/10.1016/j.jclepro.2019.118976>
- Garitaonandia I, Fernandes MH, Albizuri J (2008) Dynamic model of a centerless grinding machine based on an updated FE model. *Int J Mach Tools Manuf* 48:832–840. <https://doi.org/10.1016/j.ijmactools.2007.12.001>
- Garitaonandia I, Fernandes MH, Hernandez-Vazquez JM, Ealo JA (2016) Prediction of dynamic behavior for different configurations in a drilling-milling machine based on substructuring analysis. *J Sound Vib* 365:70–88. <https://doi.org/10.1016/j.jsv.2015.12.012>
- Liang Y, Chen W, Bai Q, Sun Y, Chen G, Zhang Q, Sun Y (2013) Design and dynamic optimization of an ultraprecision diamond flycutting machine tool for large KDP crystal machining. *Int J Adv Manuf Technol* 69:237–244. <https://doi.org/10.1007/s00170-013-5020-z>
- Shen L, Ding X, Li T, Kong X, Dong X (2019) Structural dynamic design optimization and experimental verification of a machine tool. *Int J Adv Manuf Technol* 104:3773–3786. <https://doi.org/10.1007/s00170-019-04049-7>
- Lin CY, Hung JP, Lo TL (2010) Effect of preload of linear guides on dynamic characteristics of a vertical column-spindle system. *Int J Mach Tools Manuf* 50:741–746. <https://doi.org/10.1016/j.ijmactools.2010.04.002>
- Brecher C, Fey M, Tenbrock C, Daniels M (2016) Multipoint constraints for modeling of machine tool dynamics. *ASME J Manuf Sci Eng* 138. <https://doi.org/10.1115/1.4031771>
- Ealo JA, Garitaonandia I, Fernandes MH, Hernandez-Vazquez JM, Muñoa J (2018) A practical study of joints in three-dimensional inverse receptance coupling substructure analysis method in a horizontal milling machine. *Int J Mach Tools Manuf* 128:41–51. <https://doi.org/10.1016/j.ijmactools.2018.02.002>
- Lee SW, Mayor R, Ni J (2006) Dynamic analysis of a mesoscale machine tool. *ASME J Manuf Sci Eng* DOI 10(1115/1):2123007
- Mahboubkhal M, Nategh MJ, Khadem SE (2008) Vibration analysis of machine tool's hexapod table. *Int J Adv Manuf Technol* 38:1236–1243. <https://doi.org/10.1007/s00170-007-1183-9>
- Huo D, Cheng K, Wardle F (2010) A holistic integrated dynamic design and modelling approach applied to the development of ultraprecision micro-milling machines. *Int J Mach Tools Manuf* 50:335–343. <https://doi.org/10.1016/j.ijmactools.2009.10.009>
- Deng C, Yin G, Fang H, Meng Z (2015) Dynamic characteristics optimization for a whole vertical machining center based on the configuration of joint stiffness. *Int J Adv Manuf Technol* 76:1225–1242. <https://doi.org/10.1007/s00170-014-6355-9>
- Liu S (2015) Multi-objective optimization design method for the machine tool's structural parts based on computer-aided engineering. *Int J Adv Manuf Technol* 78:1053–1065. <https://doi.org/10.1007/s00170-014-6700-z>
- Li W, Li B, Yang J (2017) Design and dynamic optimization of an ultra-precision micro grinding machine tool for flexible joint blade machining. *Int J Adv Manuf Technol* 93:3135–3147. <https://doi.org/10.1007/s00170-017-0729-8>
- Liu J, Ou Y (2019) Dynamic axial contact stiffness analysis of position preloaded ball screw mechanism. *Adv Mech Eng* 11:1687814018819289. <https://doi.org/10.1177/1687814018819289>

20. Chen H, Tan Z, Tan F, Yin G (2020) Dynamic performance analysis and optimization method of the horizontal machining center based on contact theory. *Int J Adv Manuf Technol* 108:3055–3073. <https://doi.org/10.1007/s00170-020-05597-z>
21. Kono D, Inagaki T, Matsubara A, Yamaji I (2013) Stiffness model of machine tool supports using contact stiffness. *Precis Eng* 37:650–657. <https://doi.org/10.1016/j.precisioneng.2013.01.010>
22. Kono D, Nishio S, Yamaji I, Matsubara A (2015) A method for stiffness tuning of machine tool supports considering contact stiffness. *Int J Mach Tools Manuf* 90:50–59. <https://doi.org/10.1016/j.ijmactools.2015.01.001>
23. Wu JSS, Chang JC, Hung JP (2007) The effect of contact interface on dynamic characteristics of composite structures. *Math Comput Simul* 74:454–467. <https://doi.org/10.1016/j.matcom.2006.07.003>
24. Yong-Sub Y, Kim YY, Choi JS, Yoo J, Lee DJ, Lee SW, Lee SJ (2008) Dynamic analysis of a linear motion guide having rolling elements for precision positioning devices. *J Mech Sci Technol* 22:50–60. <https://doi.org/10.1007/s12206-007-1006-9>
25. Vicente DA, Hecker RL, Villegas FJ, Flores GM (2012) Modeling and vibration mode analysis of a ball screw drive. *Int J Adv Manuf Technol* 58:257–265. <https://doi.org/10.1007/s00170-011-3375-6>
26. Dadalau A, Groh K, Reuß M, Verl A (2012) Modeling linear guide systems with CoFEM: equivalent models for rolling contact. *Prod Eng* 6:39–46. <https://doi.org/10.1007/s11740-011-0349-3>
27. Wu JSS, Chang JC, Tsai GA, Lin CY, Ou FM (2012) The effect of bending loads on the dynamic behaviors of a rolling guide. *J Mech Sci Technol* 26:671–680. <https://doi.org/10.1007/s12206-011-1228-8>
28. Brecher C, Fey M, Bäuml S (2013) Damping models for machine tool components of linear axes. *CIRP Ann* 62:399–402. <https://doi.org/10.1016/j.cirp.2013.03.142>
29. Jang WY, Park MY, Kim JH, Kang EG, Jeong JI (2017) Analysis of vibration characteristics of one-axis heavy duty stages. *J Mech Sci Technol* 31:5721–5727. <https://doi.org/10.1007/s12206-017-1113-1>
30. Yang H, Wang Z, Zhang T, Du F (2020) A review on vibration analysis and control of machine tool feed drive systems. *Int J Adv Manuf Technol* 107:503–525. <https://doi.org/10.1007/s00170-020-05041-2>
31. Allemang RJ, Brown DL (1982) A correlation coefficient for modal vector analysis. *Proceedings of the 1st international modal analysis conference*, 110–116.

Publisher's Note Springer Nature remains neutral with regard to jurisdictional claims in published maps and institutional affiliations.